

RESEARCH OUTPUTS / RÉSULTATS DE RECHERCHE

Near-Infrared BODIPY-Acridine Dyads Acting as Heavy-Atom-Free Dual-Functioning Photosensitizers

Deckers, Jasper; Cardeynaels, Tom; Penxten, Huguette; Ethirajan, Anitha; Ameloot, Marcel; Kruk, Mikalai; Champagne, Benoît; Maes, Wouter

Published in:
Chemistry: A European Journal

DOI:
[10.1002/chem.202002549](https://doi.org/10.1002/chem.202002549)

Publication date:
2020

[Link to publication](#)

Citation for pulished version (HARVARD):

Deckers, J, Cardeynaels, T, Penxten, H, Ethirajan, A, Ameloot, M, Kruk, M, Champagne, B & Maes, W 2020, 'Near-Infrared BODIPY-Acridine Dyads Acting as Heavy-Atom-Free Dual-Functioning Photosensitizers', *Chemistry: A European Journal*, vol. 26, no. 66, pp. 15212-15225. <https://doi.org/10.1002/chem.202002549>

General rights

Copyright and moral rights for the publications made accessible in the public portal are retained by the authors and/or other copyright owners and it is a condition of accessing publications that users recognise and abide by the legal requirements associated with these rights.

- Users may download and print one copy of any publication from the public portal for the purpose of private study or research.
- You may not further distribute the material or use it for any profit-making activity or commercial gain
- You may freely distribute the URL identifying the publication in the public portal ?

Take down policy

If you believe that this document breaches copyright please contact us providing details, and we will remove access to the work immediately and investigate your claim.

■ Photosensitizers

Near-Infrared BODIPY-Acridine Dyads Acting as Heavy-Atom-Free Dual-Functioning Photosensitizers

Jasper Deckers,^[a, b] Tom Cardeynaels,^[a, b, c] Huguette Penxten,^[a] Anitha Ethirajan,^[b, d] Marcel Ameloot,^[e] Mikalai Kruk,^[f] Benoît Champagne,^[c] and Wouter Maes^{*,[a, b]}

Abstract: Boron dipyrromethene (BODIPY) dyes represent a particular class within the broad array of potential photosensitizers. Their highly fluorescent nature opens the door for theragnostic applications, combining imaging and therapy using a single, easily synthesized chromophore. However, near-infrared absorption is strongly desired for photodynamic therapy to enhance tissue penetration. Furthermore, singlet oxygen should preferentially be generated without the incorporation of heavy atoms, as these often require additional synthetic efforts and/or afford dark cytotoxicity. Solu-

tions for both problems are known, but have never been successfully combined in one simple BODIPY material. Here, we present a series of compact BODIPY-acridine dyads, active in the phototherapeutic window and showing balanced brightness and phototoxic power. Although the donor–acceptor design was envisioned to introduce a charge transfer state to assist in intersystem crossing, quantum-chemical calculations refute this. Further photophysical investigations suggest the presence of exciplex states and their involvement in singlet oxygen formation.

Introduction

To date, thera(g)nostics represent an auspicious concept toward personalized cancer treatment.^[1] The concept implies the combination of diagnosis and a therapeutic approach of the cancerous disease in order to localize the target, monitor the therapeutic outcome as well as to improve drug dosimetry.^[2] One such a theragnostic platform is the combination of fluorescence bioimaging and photodynamic therapy (PDT).^[3]

Established already in 1903, PDT is nowadays a well-recognized and successful method, which has been clinically approved by the FDA more than two decades ago.^[4] Herein, light of a specific wavelength is absorbed by a photosensitizer (PS) to achieve an electronically excited singlet state (S_n) (Figure 1). Intersystem crossing (ISC) to a long-living triplet state (T_n) enables to produce different reactive oxygen species (ROS) via two possible pathways.^[5] Whereas the type I mechanism considers the interaction of the excited PS with the substrate or solvent, thereby producing a variety of ROS, the type II mechanism involves transfer of energy of the excited triplet state directly to molecular oxygen (3O_2) to produce singlet oxygen (1O_2). The ratio of both mechanisms depends on the characteristics of the PS, the substrate and the amount of available oxygen, but 1O_2 is assumed to be the main cytotoxic agent.^[6] It attacks different cellular targets, including nuclei, plasma membranes, mitochondria, and lysosomes, resulting in cell death by necrosis or apoptosis, immune responses, or vascular shutdown.^[7] PDT has several advantages, such as being noninvasive, repeatable, and affording low systemic toxicity and minimal side effects.^[8] Even more, the combination of careful illumination of the cancerous cells and the high reactivity, short lifetime, and slow diffusion rate of 1O_2 in biological media opens up the possibility for a very selective treatment.^[9] Thanks to these advantages, PDT is used for the treatment of a wide scope of tumors.^[10] In addition, the technique is frequently applied for treatment of dermatological and ophthalmic diseases, inactivation of viruses, and to treat bacterial or fungal infections.^[4a, 10b, 11]

The ideal PS is stable, has a high molar extinction coefficient ($\epsilon > 20\,000\text{--}30\,000\text{ M}^{-1}\text{ cm}^{-1}$), a sufficiently high singlet oxygen quantum yield ($\phi_{^1O_2}$), a low dark cytotoxicity, and is easily syn-

[a] J. Deckers, T. Cardeynaels, H. Penxten, Prof. W. Maes
UHasselt-Hasselt University, Institute for Materials Research (IMO)
Design & Synthesis of Organic Semiconductors (DSOS)
Agoralaan, 3590 Diepenbeek (Belgium)
E-mail: wouter.maes@uhasselt.be


[b] J. Deckers, T. Cardeynaels, Prof. A. Ethirajan, Prof. W. Maes
IMEC, Associated Lab IMOMECE
Wetenschapspark 1, 3590 Diepenbeek (Belgium)

[c] T. Cardeynaels, Prof. B. Champagne
UNamur-University of Namur, Laboratory of Theoretical Chemistry (LTC)
Theoretical and Structural Physical Chemistry Unit
Namur Institute of Structured Matter, Rue de Bruxelles 61
5000 Namur (Belgium)

[d] Prof. A. Ethirajan
UHasselt-Hasselt University, Institute for Materials Research (IMO)
Nano-Biophysics and Soft Matter Interfaces (NSI)
Wetenschapspark 1, 3590 Diepenbeek (Belgium)

[e] Prof. M. Ameloot
UHasselt-Hasselt University, Biomedical Research Institute (BIOMED)
Agoralaan, 3590 Diepenbeek (Belgium)

[f] Prof. M. Kruk
Belarusian State Technological University
Sverdlov Str., 13a, 220006, Minsk (Belarus)

 Supporting information and the ORCID identification number(s) for the author(s) of this article can be found under:
<https://doi.org/10.1002/chem.202002549>

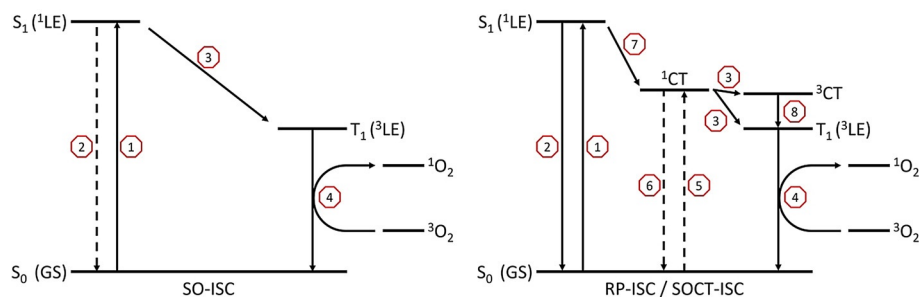


Figure 1. Energy diagrams presenting the principle of spin-orbit intersystem crossing (SO-ISC, left) and radical pair intersystem crossing or spin-orbit exciplex intersystem crossing (RP-ISC, SOCT-ISC, right). The different photophysical processes are indicated with red octagons: 1) localized absorption, 2) localized emission, 3) intersystem crossing (SO-ISC: $^1LE \rightarrow ^3LE$, RP-ISC: $^1LE \rightarrow ^3CT$, SOCT-ISC: $^1CT \rightarrow ^3LE$), 4) energy transfer to molecular oxygen, 5) charge transfer absorption, 6) charge transfer emission, 7) photoelectron transfer, and 8) internal conversion.

thesized.^[8] The activation energy of the PS is important as well. Before the applied light reaches the target tumor, it will be scattered and absorbed by the surrounding tissue.^[12] Shorter wavelengths are absorbed by different tissue chromophores and often give rise to skin photosensitivity.^[6] To minimize these effects, longer wavelengths are desirable for PS activation. In this way, light scattering is reduced, the background signal from autofluorescence of biomolecules is minimized, and the penetration depth is strongly enhanced.^[13] As water absorption becomes significant above 1300 nm, the area between 600 and 1200 nm is referred to as the “optical window” of biological tissue.^[14] However, wavelengths above 800 nm lack energy to generate 1O_2 , since the associated triplet state would be too low in energy.^[15] In this respect, the phototherapeutic area in the near-infrared (NIR) region ($\approx 600\text{--}800\text{ nm}$) has triggered a lot of interest.^[13] Most synthetic and naturally occurring PSs (whether or not satisfying the aforementioned ideal characteristics) are oligopyrrolic macrocycles, but a broad scope of other structures are widely studied as well.^[6,16] The majority of the (pre)clinical stage PSs are derivatives of porphyrins, such as Photofrin, Tookad, and NPe6.^[169] Although showing several advantages, these compounds are often correlated to dark cytotoxicity, prolonged skin photosensitivity, and other side effects, explaining the increased interest in non-porphyrinic PSs.^[17]

Recently, 4,4-difluoro-4-bora-3a,4a-diaza-s-indacenes or boron dipyrromethenes (BODIPYs) have been added to the arsenal of cancer theragnostic materials.^[18] Often referred to as porphyrin's little sister, BODIPY dyes possess many characteristics to be suitable PSs. These compounds have high molar extinction coefficients, a high chemical and photochemical stability, and are easily modified, allowing to fine-tune their photophysical properties.^[19] Even more, due to its restricted flexibility, the BODIPY core inherently affords high fluorescent quantum yields (ϕ_f) and a narrow emission profile, interesting characteristics for the development of a dual-functioning PS. However, there are two main shortcomings. First, unmodified BODIPY dyes have their absorption and emission peaks around 500 nm. Luckily, a broad scope of structural modifications to the BODIPY core are known to afford NIR activity.^[20] The second, even more important, problem is the lack of ability to generate 1O_2 from BODIPY dyes due to the very poor triplet formation yields. The most common solution is the introduc-

tion of bromine, iodine, or transition metal complexes.^[18,21] Thanks to spin-orbit coupling (SOC), this induces increased ISC through the heavy-atom effect.^[22] In this regard, a vast amount of NIR photoactive aza-, styryl-, and other BODIPY PSs are known.^[18,21] However, this approach turned out to be far from ideal as these heavy atoms are correlated to a shortening of the triplet state lifetimes, increased dark cytotoxicity, and additional synthetic efforts and related costs.^[23] Moreover, fluorescence signals are quenched almost completely when a high ϕ_A is reached, since ISC and fluorescence are competing pathways for the excited state. Aiming at dual-functioning PSs with both a significant 1O_2 production and fluorescence quantum yield, these problems necessitate the search for alternative methods to achieve a balanced (molecular) brightness (BT , product of ϵ and ϕ_f) and phototoxic power (PP , product of ϵ and ϕ_A).

Some alternative methods to increase triplet populations without relying on the heavy-atom effect have emerged, such as radical enhanced ISC, the use of a spin converter, and charge recombination induced ISC.^[24] In this regard, halogen-free BODIPY PSs were designed over the past few years.^[21,25] However, radical enhanced ISC and C_{60} spin converters quench the fluorescence, while the synthetic effort and related costs increase.^[26] Another example are thienopyrrole-fused BODIPYs, but the triplet formation seems intrinsic to this system.^[27] Recently, photoinduced electron transfer (PET) was applied to donor–acceptor BODIPY dyads and dimers to successfully obtain controllable triplet states and ϕ_f .^[25] In PET, electron transfer or charge separation after light absorption results in the occupation of a highly polar excited state, that is, a charge transfer (CT) or charge separated state (CSS).^[28] This 1CT state can undergo charge recombination into a triplet state, thereby rendering heavy atoms unnecessary for 1O_2 generation.^[29] Depending on the molecular structure, two different charge recombination induced ISC mechanisms can be distinguished: radical pair ISC (RP-ISC) and spin-orbit charge transfer ISC (SOCT-ISC).^[24c,25] The former is more pronounced when there is a large separation distance between the donor and acceptor parts of the PS, resulting in a weak electronic coupling. This process involves the formation of an intermediate triplet CT state (3CT) via hyperfine interaction, followed by fast charge recombination into the localized triplet (3LE) state. The second mechanism is found in dyads and dimers with a small spacer

or no spacer at all between both moieties. SOCT-ISC becomes possible if the ^1CT - ^3LE energy difference is small and the ^1CT state is converted into a ^3LE state through back-electron transfer and spin conversion. To visualize the difference between traditional PDT based on SO-ISC and the heavy-atom-free RP-ISC and SOCT-ISC mechanisms, simplified energy diagrams are provided in Figure 1. There are some examples of compact BODIPY dimers and dyads that successfully combine fluorescence and $^1\text{O}_2$ production through this mechanism.^[24] However, to the best of our knowledge, there are no previous examples of BODIPY PSs wherein $^1\text{O}_2$ is obtained efficiently together with a significant ϕ_f when irradiated in the phototherapeutic window. There is one particular example reported by Ortiz and co-workers, who synthesized an orthogonal BODIPY dimer whereby one of the two BODIPY units is modified with two styryl groups at the α -positions.^[30] Although having absorption maxima at 509 and 658 nm, and a fluorescence maximum at 685 nm ($\phi_f=0.56$), $^1\text{O}_2$ generation ($\phi_d=0.11$) was only observed when the system was excited using green light. This indicates that triplet formation is occurring in the non-altered BODIPY unit, whereas this is hampered in the π -extended BODIPY unit. It seems that enlarging the delocalized area enhances the radiative processes from the CT state, thereby hindering the ISC for triplet formation.

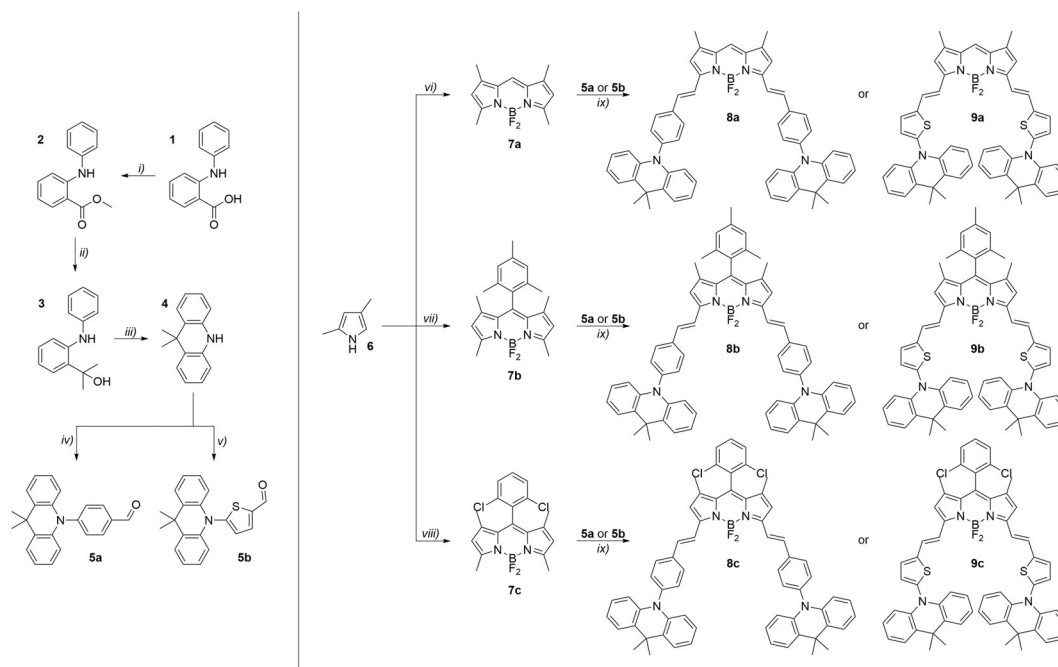
In this manuscript, we present a series of novel dual-functioning BODIPY PSs showing a reasonably high $^1\text{O}_2$ production, while maintaining satisfying fluorescent abilities, all within the phototherapeutic window. We started from different highly fluorescent 1,3,5,7-tetramethyl-BODIPY cores and shifted the

absorption and emission to the NIR region through a simple Knoevenagel-type condensation of the α -methyl groups. In accordance with the idea of an SOCT-ISC mechanism, acridine moieties were attached to provide an orthogonal donor-acceptor design. Density functional theory (DFT) was used to investigate the BODIPY dye geometries and frontier molecular orbitals. Extensive photophysical characterization of the dyads was performed in different solvents and the influence of the incorporated dimethylacridine end groups was examined. Although these photophysical data at first sight seemed to match with the idea of a CT state being involved, time-dependent (TD) DFT calculations starting from the ground state geometries did not confirm this mechanism. Further investigations unveiled the probable presence of “exciplexes”^[31] in these systems. As their nature is similar to the highly polar CT state, they could also play an important role in singlet oxygen formation.^[32] Since exciplex singlet and triplet states are close to each other in energy, they serve the same purpose as the CT energy levels depicted in Figure 1, thereby assisting triplet formation.

Results and Discussion

Structural design and synthesis

The design of the PSs started from the highly fluorescent 1,3,5,7-tetramethyl-BODIPYs **7a–c**, as depicted in Scheme 1. The methyl groups are acidic enough to enable Knoevenagel-type condensations to extend the π -conjugated system.^[33] The



Scheme 1. Synthesis of the BODIPY PSs and their building blocks: i) thionyl chloride, methanol, 0 °C; 16 h at 60 °C (77 %); ii) methylmagnesium bromide, dry THF, −78 °C; 12 h at RT (92 %); iii) H_3PO_4 , 2 h at 35 °C (75 %); iv) 4-bromobenzaldehyde, $\text{Pd}_2(\text{dba})_3$, Cs_2CO_3 , dppf, dry toluene, inert atm, 16 h at 100 °C (91 %); v) 5-bromothiophene-2-carbaldehyde, $\text{Pd}(\text{OAc})_2$, NaBuO , XPhos, dry toluene, inert atm, 16 h at 100 °C (61 %); vi) triethoxymethane, trifluoroacetic acid, dry CH_2Cl_2 , inert atm, 2 h at RT; Et_3N , $\text{BF}_3\cdot\text{OEt}_2$, dry toluene, 1 h at RT (47 %); vii) 2,4,6-trimethylbenzaldehyde, trifluoroacetic acid, dry CH_2Cl_2 , inert atm, 3 h at 0 °C; DDQ, 20 min at 0 °C, 1 h at RT; Et_3N , $\text{BF}_3\cdot\text{OEt}_2$, 12 h at RT (72 %); viii) 2,6-dichlorobenzaldehyde, trifluoroacetic acid, dry CH_2Cl_2 , inert atm, 1 h at RT; DDQ, 10 min at 0 °C, 1 h at RT; Et_3N , $\text{BF}_3\cdot\text{OEt}_2$, 2 h at RT (23 %); ix) glacial acetic acid, piperidine, dry DMF, inert atm, 5 min at 150 °C, microwave irradiation (40–66 %).

introduction of vinyl groups provides a direct and easy way to obtain bathochromically shifted absorption and emission features. We chose for a strongly electron donating acridine end group, as often applied for materials displaying thermally activated delayed fluorescence (TADF).^[34] Because the BODIPY core is relatively electron deficient, the introduction of an electron donating group via Knoevenagel condensation generates a push-pull type structure, further increasing the bathochromic shift. This donor–acceptor dyad design was supposed to introduce the desired CT state required for efficient ISC.^[24c] Although the exact structural requirements for SOCT-ISC are still not very well understood, orthogonality between the BODIPY core and the rest of the structure is suggested to support this process as the change in molecular orbital angular momentum will compensate for the change in electron spin angular momentum during ISC, hence slowing down the charge recombination process to the ground state and enhancing triplet formation.^[29a] In our design, the C–N induced torsion between the donor and acceptor part is hence an essential aspect.

Three different BODIPY cores with varying *meso*-groups—hydrogen (**7a**), mesityl (**7b**), and 2,6-dichlorophenyl (**7c**)—were synthesized according to literature procedures starting from 2,4-dimethylpyrrole (**6**).^[35] Dimethylacridine **4** was obtained through a three-step synthesis from *N*-phenylanthranilic acid (**1**) with a good overall yield of 53%. As an aldehyde functionality is needed for the Knoevenagel condensation, a spacer should be introduced between the donor and acceptor moiety. To screen two spacer types in the target PSs, dimethylacridine **4** was subjected to a Buchwald–Hartwig amination with either 4-bromobenzaldehyde or 5-bromothiophene-2-carbaldehyde. The thienyl spacer was envisioned to provide an additional small red-shift. First tests were performed using Pd₂(dba)₃ and BINAP, but without success. When using Pd(OAc)₂ and P(*t*Bu)₃HBf₄, aldehydes **5a** and **5b** were obtained in moderate yields (33 and 43%, respectively). Further optimization was performed using Pd(OAc)₂ in combination with XPhos, increasing the yields to 54 and 61%, respectively. Eventually, we were able to maximize the yield of **5a** to 91% using Pd₂(dba)₃ and 1,1'-bis(diphenylphosphino)ferrocene (dppf) as the catalytic system.

The Knoevenagel condensation itself was initially optimized for BODIPY **8b**, as summarized in Table 1. The condensation of an aldehyde with a methyl group at the BODIPY 3- and 5-positions is well-known.^[20] However, refluxing in benzene overnight in the presence of 3 Å molecular sieves did not result in the target product. A switch was made to microwave irradiation, yielding 36% of BODIPY **8b** in only 5 minutes. Further optimization pointed out that a higher concentration is preferred (entries 3 and 5), a longer reaction time results in more degradation (entry 4), more equivalents of benzaldehyde push the reaction to the right (entry 6), and a temperature of 150 °C is ideal to increase the conversion (entries 6 to 8). Finally, the optimal reaction conditions were used to combine aldehydes **5a** and **5b** with BODIPYs **7a–c** to obtain six different π -extended BODIPY dyes. Three of them, BODIPYs **8a–c**, bear a phenyl spacer between the BODIPY core and the acridine moiety, while dyads **9a–c** are equipped with a thienyl spacer. Reactions with BODIPY **7a** were performed with only three equivalents of aldehydes **5a,b** as tri- and tetra-substitution was observed to a larger extent, likely due to the lack of a sterically hindering group at the *meso*-position. In the end, good yields ranging from 40 to 66% were obtained for all final products. Dyads **8a–c** have a blue color in solution, while BODIPYs **9a–c** give a green solution, thereby already indicating a variation in spectroscopic properties due to the different spacer. For a detailed description of the synthesis protocols, we refer to the Supporting Information.

Structural analysis

To confirm our design objectives, DFT was used to optimize the ground state geometries of BODIPYs **8a–c** and **9a–c** in three different solvents with varying polarity (toluene, chloroform, and dimethyl sulfoxide (DMSO)) using the polarizable continuum solvation model (PCM).^[36] All vibrational frequencies are real, demonstrating the optimized geometries correspond to minima on the potential energy surface. From the optimized geometries in chloroform (Figure 2 and Figure 3), a large dihedral angle ($\theta > 80^\circ$) between the donor (acridine) and acceptor (styryl/thienylvinyl-BODIPY) units can be seen.

Table 1. Optimization of the Knoevenagel-type condensation toward BODIPY **8b**.^[a,b]

Entry	Equiv 7b	Equiv 5a	Temperature [°C]	Reaction time [min]	Solvent volume [mL mmol ⁻¹]	Yield ^[c] 8b-mono ^[d]	Yield ^[c] 8b	Remnant ^[c] 7b
1	1	3	80	960	200	0%	0%	— ^[e]
2	1	3	150	5	240	7%	36%	— ^[e]
3	1	3	150	5	120	7%	46%	44%
4	1	3	150	15	120	9%	46%	27%
5	1	3	150	5	60	6%	53%	34%
6	1	4	150	5	60	9%	66%	23%
7	1	4	175	5	60	11%	51%	10%
8	1	4	125	5	60	17%	45%	35%

[a] All reactions were done on a 0.1 mmol scale, except for entries 1 and 2, which were done on a 0.05 mmol scale. [b] Experimental conditions for entry 1: 0.05 mL glacial acetic acid, 0.05 mL piperidine, 3 Å molecular sieves, benzene, inert atmosphere, reflux. Experimental conditions for entries 2 to 8: 0.1 mL glacial acetic acid, 0.1 mL piperidine, dry DMF, inert atmosphere, microwave irradiation, 1 min pre-stirring. [c] All reported yields are isolated yields. [d] Monostyryl side product of distyryl-BODIPY **8b**. [e] Not isolated.

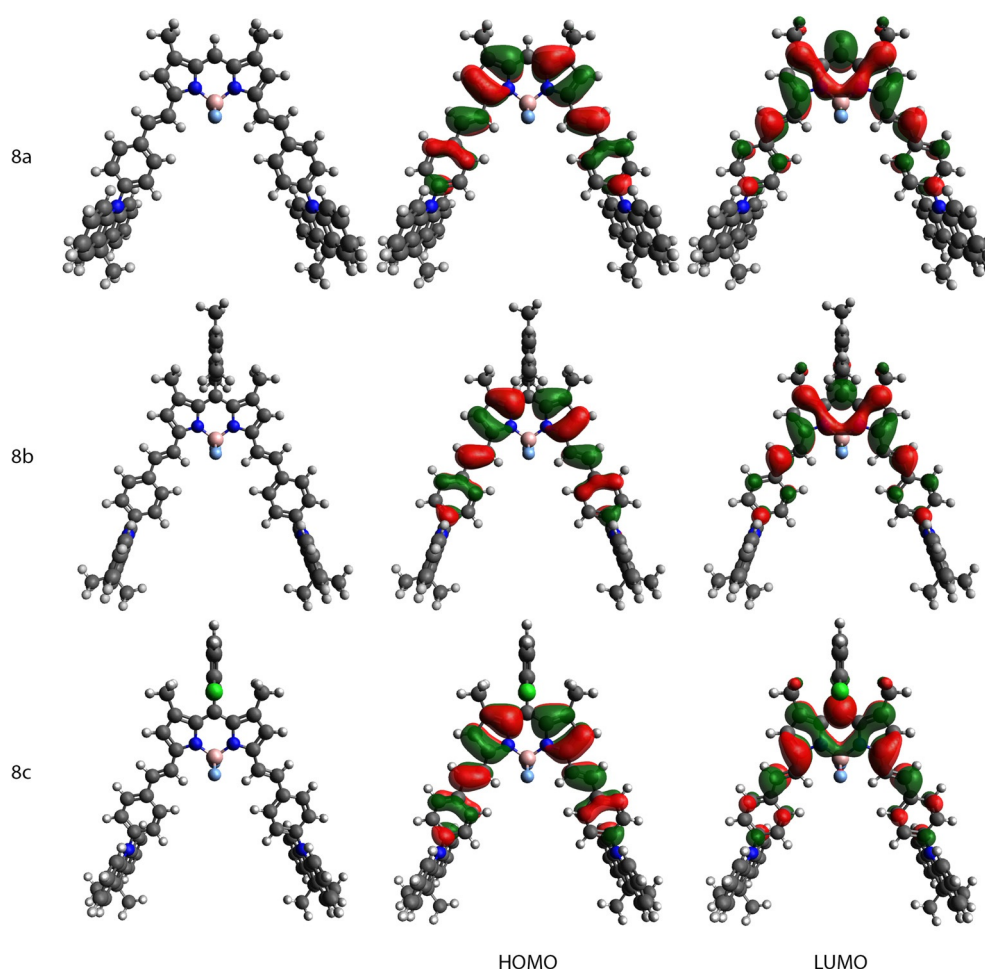


Figure 2. Optimized geometries and frontier orbitals for BODIPYs **8a–c** in chloroform solution obtained using DFT calculations with M06-2X/6–311G(d) and the PCM model. Isosurface values of 0.02 (a.u.) were used for all orbitals.

The phenyl and thienyl spacers are coplanar with the BODIPY core, thus extending the conjugation. For all BODIPYs, the highest occupied molecular orbital (HOMO) and lowest unoccupied molecular orbital (LUMO) reside on the styryl/thienylvinyl BODIPY system. The HOMO–1 and HOMO–2 can be found on the acridine units, while the HOMO–3 is again found on the styryl/thienylvinyl BODIPY core (Figures S1 and S2 in the Supporting Information). The mesityl and 2,6-dichlorophenyl *meso*-groups in **8b/9b** and **8c/9c**, respectively, are nearly perpendicular to the rest of the BODIPY core and almost completely electronically decoupled. Therefore, these groups are not expected to influence the experimental and calculated energy levels to a large extent. The geometries and frontier orbital topologies are similar in toluene and DMSO.

Photophysical characterization

The six heavy-atom-free potential BODIPY PSs were subjected to a detailed photophysical characterization to examine their intended use as theragnostic agents. Initial photophysical characterization of BODIPY dyes **8a–c** and **9a–c** was performed in chloroform solution. Absorption and emission spectra afforded the spectral maxima ($\lambda_{abs}(max)$, $\lambda_{em}(max)$), Stokes shifts ($\Delta\bar{\nu}$),

and the full-width-at-half-maximum ($fwhm_{abs}$, $fwhm_{em}$) of both the emission and absorption bands. Fluorescence quantum yields (ϕ_f) were obtained relative to a suitable reference dye and using the corresponding excitation wavelengths. Singlet oxygen quantum yields (ϕ_{Δ}) were collected by monitoring the absorbance of 1,3-diphenylisobenzofuran (1,3-DPBF) as singlet oxygen scavenger during excitation at 639 nm (Figure S4).^[37] In combination with the molar attenuation coefficient (ϵ), the brightness (BT) and phototoxic power (PP) have been determined. All data represented in Figure 4 and Table 2 are mean values which originate from three independent measurements for each compound. Only data from the wavelength region of interest are displayed here. For the full absorption spectra, we refer to Figure S3 and Table S2. Furthermore, all systems were found to be photostable for more than three hours under 639 nm illumination.

For styryl-BODIPYs **8a–c**, introduction of the acridine-styryl groups resulted in a bathochromic shift of around 140 nm for the absorption maximum with respect to the starting BODIPY cores **7a–c**. The fluorescence maxima change in the same manner, retaining the small Stokes shift characteristic of BODIPY dyes. As such, these three materials are active in the targeted phototherapeutic window. The ϕ_f values decrease, as

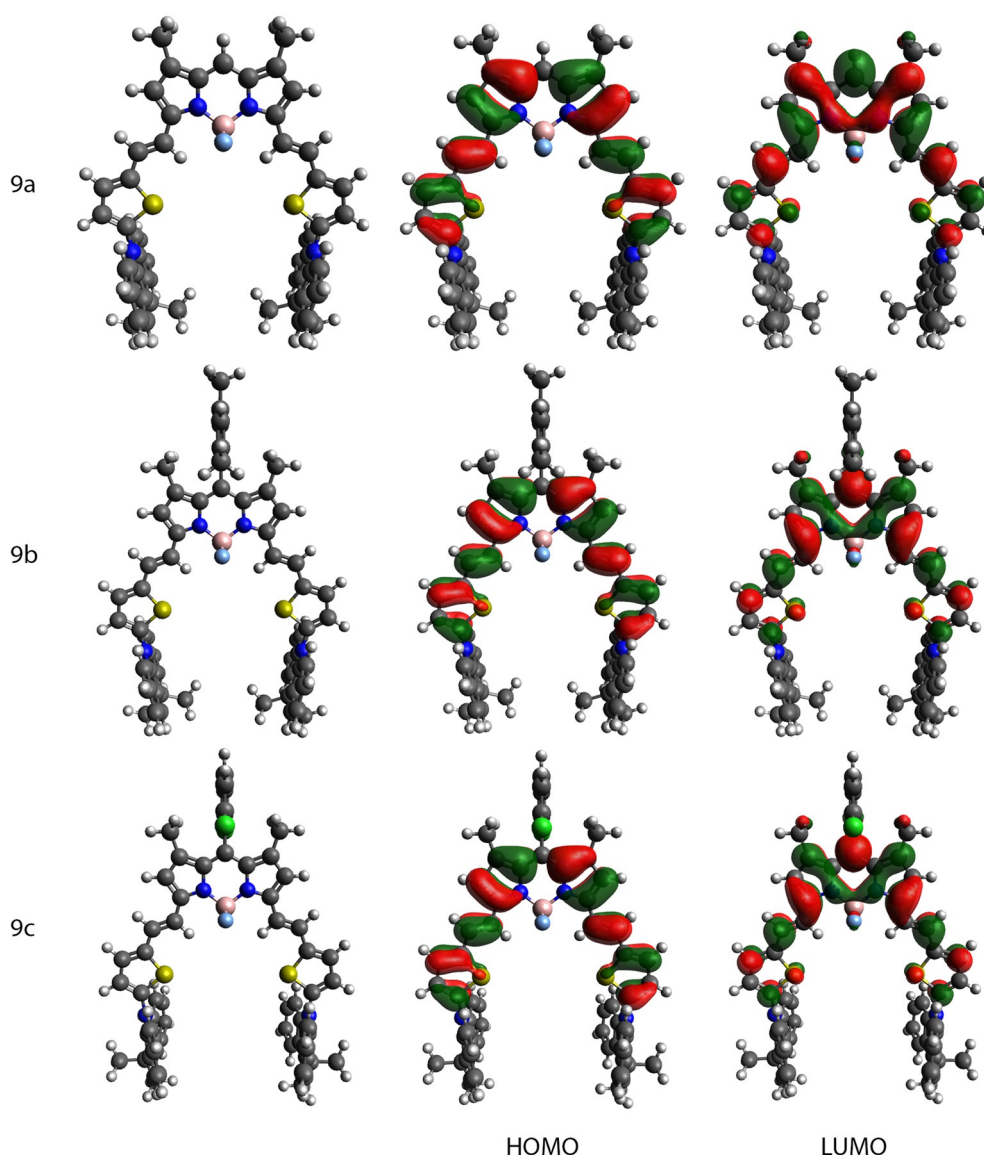


Figure 3. Optimized geometries and frontier orbitals for BODIPYs **9a–c** in chloroform solution obtained using DFT calculations with M06-2X/6-311G(d) and the PCM model. Isosurface values of 0.02 (a.u.) were used for all orbitals.

expected for red-shifted dyes due to the energy-gap law, but are still significant (47, 63, and 38% for **8a**, **8b**, and **8c**, respectively). Both the absorption and emission profiles resemble the typical narrow BODIPY shape with a smaller shoulder. To our delight, the BODIPY dyads with a phenyl spacer between the BODIPY and acridine subunits were able to generate $^1\text{O}_2$ when irradiated using a 639 nm LED. Relative ϕ_{Δ} measurements were performed, resulting in good values ranging from 23% for the *meso*-mesityl variant **8b** to 31% for the *meso*-2,6-dichlorophenyl variant **8c**. We can exclude that the $^1\text{O}_2$ generation capability originates from the orthogonality between the *meso*-group and the BODIPY core, since *meso*-unsubstituted BODIPY **8a** also affords a significant ϕ_{Δ} value of 29%. Moreover, the high molar attenuation coefficients (above 100 000) indicate their excellent light harvesting abilities. This results in high and balanced *BT* and *PP* values, enabling the use of these dyes for combined bio-imaging and photodynamic therapy.

The absorption profiles of BODIPYs **9a–c** resemble those of their styryl counterparts, but are red-shifted to a greater extent, as expected due to the more electron donating character of the thienyl linkers. Bathochromic shifts up to 170 nm with respect to BODIPYs **7a–c** are observed, bringing the absorption deeper into the NIR. An additional, small absorption band is seen around 740 nm. Remarkably, the thienyl spacer results in a very different fluorescence emission profile. The first emission maxima are found between 680 and 700 nm, corresponding to small Stokes shifts. However, a second, more intense and broad emission band with maxima ranging from 750 up to 780 nm appears. Although high molar attenuation coefficients are obtained for these systems, ϕ_f and ϕ_{Δ} values are found to be very low. Clearly, dyads **9a–c** behave very differently with respect to the distyryl analogues **8a–c**, making them unsuitable as dual PSs.

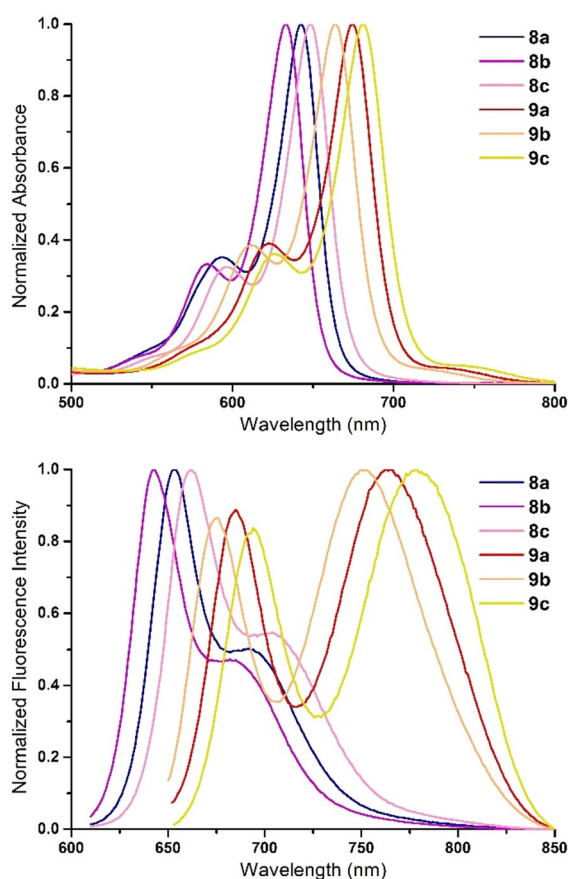


Figure 4. Normalized absorption spectra of BODIPYs **8a–c** and **9a–c** (top) and their corresponding normalized fluorescence emission spectra (bottom) in chloroform solution.

Elucidation of the spectral differences

To get an idea on the origin of the observed spectral differences, the nature of the second emission band observed for

molecules **9a–c** was investigated in more detail. Since the dyads were designed to form an intramolecular CT state, this was examined first. A possible explanation for the lack of fluorescence and phototoxicity for **9a–c** could be the (non-)radiative charge recombination from the CT state to the ground state. The combination of non-radiative losses and restricted triplet formation would result in the observed low ϕ_f and ϕ_d values.

To verify the CT character of the lowest energy fluorescence band in BODIPY dyads **9a–c**, and the possible involvement of a CT band in the efficient ISC for **8a–c**, the effect of solvent polarity on the absorption and emission profiles was investigated. When increasing solvent polarity, the highly polar CT state is stabilized, resulting in a bathochromic shift and broadening of the CT band, accompanied with a decrease in ϕ_f .^[38] However, the CT state is not always visible through its emission, as it could also undergo non-radiative charge recombination to the ground state or recombination into a triplet state, depending on the polarity of the medium.^[29] BODIPYs **8a–c** and **9a–c** were hence subjected to the same photophysical characterization as performed in chloroform ($E_T(30)=39.1$), but now in the more nonpolar solvent toluene ($E_T(30)=33.9$) and the more polar solvent DMSO ($E_T(30)=45.1$).^[39] Normalized absorption and emission spectra are given in Figure 5. Here, the profiles are grouped by BODIPY PS in different solvents to more clearly visualize the influence of polarity changes. The extracted data from three independent measurements in each solvent are summarized in Table S3. Only data from the wavelength region of interest are displayed here. For the complete absorption spectra in each solvent, we again refer to Figure S3 and Table S2. The monitored decrease of 1,3-DPBF absorption during $^1\text{O}_2$ measurements in each solvent is also illustrated in Figure S4.

The absorption maxima and profiles of PSs **8a–c** are not influenced to a large extent by solvent polarity, indicating an unaffected localized singlet (^1LE) energy in different solvents.

Table 2. Spectroscopic data for BODIPY dyads **8a–c** and **9a–c** as obtained in chloroform solution.^[a]

BODIPY	λ_{abs} [nm] ^[b]	λ_{em} [nm] ^[c]	$\Delta\bar{\nu}$ [cm ^{−1}] ^[d]	fwhm_{abs} [cm ^{−1}] ^[e]	fwhm_{em} [cm ^{−1}] ^[f]	ϵ [M ^{−1} cm ^{−1}] ^[g]	ϕ_f ^[h]	ϕ_d ^[i]	BT [M ^{−1} cm ^{−1}] ^[j]	PP [M ^{−1} cm ^{−1}] ^[k]
8a	643	654	270	748	883	122 300	0.47 ± 0.02	0.29 ± 0.04	57 600	33 100
8b	633	645	294	777	917	119 900	0.63 ± 0.03	0.23 ± 0.02	75 200	27 800
8c	648	664	379	768	1431	100 100	0.38 ± 0.02	0.31 ± 0.07	38 200	30 400
9a	674	689 764	316	767	793, 1154	107 300	0.069 ± 0.002	0.03 ± 0.01	7400	2600
9b	664	678 751	311	805	768 1190	98 200	0.091 ± 0.002	0.05 ± 0.03	9000	6000
9c	681	697 782	344	781	743 1111	98 400	0.052 ± 0.002	0.06 ± 0.04	5100	5200

[a] Spectrograde chloroform was used for all measurements. All values are averages from three independent measurements. [b] Absorption maximum. [c] Fluorescence emission maximum/maxima. [d] Stokes shift between the localized absorption and emission maxima. [e] Full-width-at-half-maximum of the absorption band. [f] Full-width-at-half-maximum of the emission band(s). [g] Molar attenuation coefficient. [h] Fluorescence quantum yield determined vs. Nile blue ($\phi_f=0.27$, $\lambda_{\text{exc}}=605$ nm) (for **8a–c**) or vs. aluminum phthalocyanine chloride ($\phi_f=0.41$, $\lambda_{\text{exc}}=645$ nm) (for **9a–c**) in spectrograde ethanol as a reference. Standard deviations are reported. [i] Singlet oxygen quantum yield determined vs. methylene blue ($\phi_d=0.52$, $\lambda_{\text{exc}}=639$ nm) in spectroscopic grade ethanol as a reference by monitoring the absorbance of 1,3-DPBF at 414 nm. Standard deviations are reported. [j] Fluorescence brightness. [k] Phototoxic power.

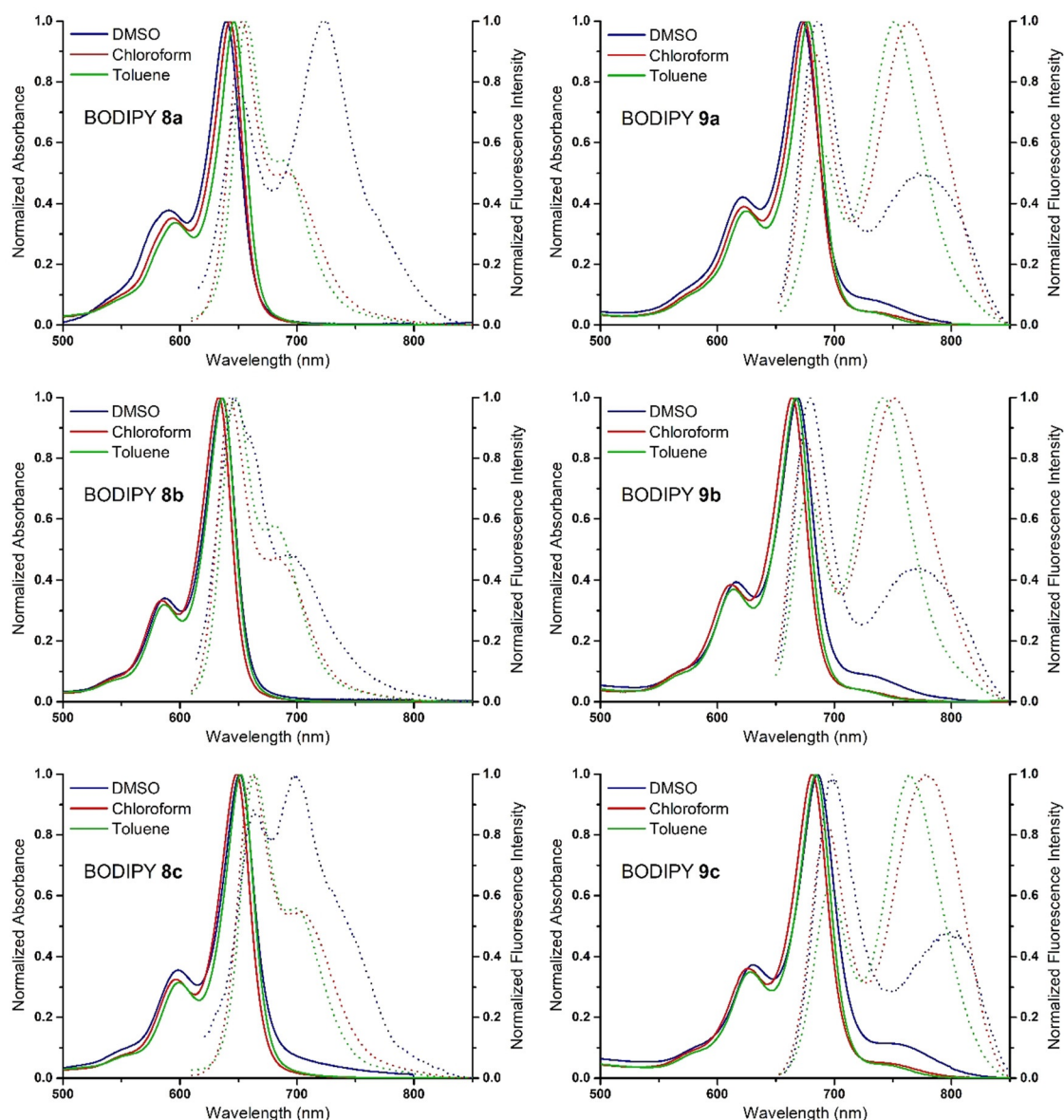


Figure 5. Normalized absorption spectra (solid lines) of BODIPYs **8a–c** and **9a–c** and their corresponding normalized fluorescence emission spectra (dashed lines) in toluene, chloroform, and DMSO.

However, the fluorescence signals are distinctly different. When going from chloroform to toluene, the localized emission peak, originating from the radiative $^1\text{LE} \rightarrow \text{S}_0$ transition, is almost identical, as expected from the rigid ^1LE state. The same can be seen in the more polar solvent DMSO, but with the arise of a second band. This red-shifted emission peak is clearly observed for BODIPY **8a** at 728 nm. It is also present in dyads **8b** and **8c**, although partially overlapping with the localized emission peak. The variable nature depending on solvent polarity suggests a CT character for these emission bands. The difference in the position of this band between the three BODIPY dyes bearing a phenyl spacer is remarkable. Whereas both emission bands are visually separated for **8a**, these bands are closer to each other in BODIPY **8c**, whereas for **8b** it is only seen as an additional broadening of the localized emission peak. This would suggest a close encounter of the ^1LE and ^1CT energy

levels in BODIPY **8b**, in contrast to the larger energy difference in **8a**. The change in solvent polarity also affects the ϕ_f and ϕ_d values (Table S3). The fluorescence capability in toluene is higher as compared to chloroform for all styryl-BODIPYs. This occurs at the expense of the $^1\text{O}_2$ generation capabilities. Surprisingly, the opposite is not the case in DMSO. In this polar solvent, both ϕ_f and ϕ_d are close to zero.

Different trends are observed when comparing the photo-physical characteristics of BODIPYs **9a–c** in toluene, chloroform, and DMSO. Concerning photon absorption, comparable absorption profiles and maxima are observed. As in chloroform, a second, although relatively weak, low-energy absorption band can also be observed in toluene and DMSO, which is not present in the **8a–c** series. Regarding the fluorescence signals, the same influence of solvent polarity was noticed for **9a**, **9b**, and **9c**. In all solvents, localized emission from the ^1LE

state is very similar. The second peaks again change in accordance to the polarity of the surrounding medium, as expected for CT emission bands. The emission maxima decrease by approximately 13 nm when going from chloroform to toluene, while a 16 nm red-shift is obtained in DMSO. The bands also broaden with increasing solvent polarity. In all solvents, fluorescence and $^1\text{O}_2$ production remain relatively low, which could be due to extensive non-radiative losses by the presence of the mobile thienyl spacer. ϕ_f values seem to increase slightly in nonpolar media, whereas ϕ_d values increase a bit in more polar environments.

From these results, it looks like CT states could be involved in all systems, although its presence is not always observed spectroscopically. To get additional confirmation, TDDFT calculations were run to verify the position and CT character of this additional energy level. Despite known issues in accurately describing the singlet and triplet excited states for BODIPY type compounds related to CT transitions, multireference character

states and double excitations,^[40] Chibani et al. showed that using M06-2X as the exchange correlation functional in TDDFT calculations on BODIPY compounds can give fairly accurate representations of the excitation energies.^[41] Furthermore, M06-2X has been found to give good estimates for the singlet and triplet excitation energies for various small molecules and donor-acceptor compounds when benchmarked versus MS-CASPT2, CC2 and CC3 calculations.^[42] Unfortunately, due to the size of the systems under investigation here, such wavefunction methods are not feasible as the computational demands are too high. Therefore, TDDFT calculations were performed at the M06-2X/6-311G(d) level to calculate the vertical excitation energies of the singlet and triplet states in toluene, chloroform, and DMSO with the PCM model (Table 3, visualized in Figure S5). The singlet excitation energies for BODIPYs **8a–c** show that **8b** has the highest first excitation energy, followed by **8a** and **8c**. This is expected given the electron donating nature of the mesityl group, whereas the 2,6-dichlorophenyl group is

Table 3. Calculated vertical singlet (S_1 and S_2) and triplet (T_1 and T_2) excitation energies and their corresponding oscillator strengths for BODIPYs **8a–c** and **9a–c**.

BODIPY	Solvent ^[a]	S ₁				S ₂			T ₁		T ₂	
		E [eV] ^[b]	λ [nm] ^[b]	Osc. Str. ^[c]	Nature ^[d]	E [eV] ^[b]	Osc. Str. ^[c]	Nature ^[d]	E [eV] ^[b]	Nature ^[d]	E [eV] ^[b]	Nature ^[d]
8a	toluene	2.17	572	1.25	H→L (98%)	2.96	0.00	H-1→L (91%)	1.05	H→L (94%)	2.51	H-3→L (49%)
	chloroform	2.18	569	1.24	H→L (98%)	3.00	0.00	H-1→L (87%)	1.06	H→L (94%)	2.51	H-3→L (48%)
	DMSO	2.19	567	1.23	H→L (97%)	3.04	0.00	H-1→L (85%)	1.07	H→L (94%)	2.51	H-3→L (48%)
8b	toluene	2.21	560	1.16	H→L (95%)	3.03	0.00	H-2→L (69%)	1.16	H→L (91%)	2.50	H-3→L (51%)
	chloroform	2.22	558	1.15	H→L (96%)	3.05	0.00	H-1→L (88%)	1.16	H→L (92%)	2.49	H-3→L (51%)
	DMSO	2.23	557	1.14	H→L (97%)	3.08	0.00	H-2→L (88%)	1.17	H→L (93%)	2.50	H-3→L (50%)
8c	toluene	2.16	573	1.19	H→L (97%)	2.93	0.00	H-2→L (91%)	1.06	H→L (93%)	2.49	H-3→L (52%)
	chloroform	2.17	571	1.18	H→L (97%)	2.95	0.00	H-2→L (84%)	1.06	H→L (94%)	2.49	H-3→L (52%)
	DMSO	2.18	569	1.17	H→L (97%)	2.96	0.00	H-2→L (83%)	1.07	H→L (94%)	2.489	H-3→L (51%)
9a	toluene	2.07	598	1.08	H→L (97%)	3.02	0.00	H-1→L (76%)	0.99	H→L (93%)	2.26	H-3→L (48%)
	chloroform	2.08	596	1.06	H→L (97%)	3.05	0.00	H-1→L (88%)	1.00	H→L (93%)	2.25	H-3→L (47%)
	DMSO	2.10	591	0.90	H→L (96%)	3.06	0.01	H-1→L (82%)	1.03	H→L (91%)	2.27	H-3→L (47%)
9b	toluene	2.12	585	1.00	H→L (97%)	3.08	0.00	H-1→L (76%)	1.10	H→L (92%)	2.25	H-3→L (49%)
	chloroform	2.13	583	0.99	H→L (97%)	3.09	0.00	H-1→L (78%)	1.10	H→L (92%)	2.25	H-3→L (49%)
	DMSO	2.13	583	0.94	H→L (97%)	3.10	0.00	H-1→L (87%)	1.10	H→L (92%)	2.24	H-3→L (48%)
9c	toluene	2.07	599	1.06	H→L (97%)	3.11	0.01	H-2→L (88%)	1.00	H→L (93%)	2.24	H-3→L (49%)
	chloroform	2.08	597	1.05	H→L (97%)	3.12	0.01	H-2→L (88%)	1.00	H→L (93%)	2.24	H-3→L (49%)
	DMSO	2.08	596	1.03	H→L (97%)	3.13	0.01	H-1→L (88%)	1.00	H→L (93%)	2.23	H-3→L (49%)

[a] Solvents are listed from top to bottom according to increasing polarity $E_T(30)$. [b] Vertical excitation energy. [c] Oscillator strength. [d] H = HOMO, L = LUMO.

slightly electron withdrawing. BODIPYs **9a–c** have lower excitation energies, in correspondence to the bathochromically shifted absorption and emission spectra. Furthermore, these compounds follow the same trend concerning variations of the *meso*-groups. In all cases, the energy differences between the different solvents are minimal, suggesting similar absorption maxima. These observations correspond nicely to the trends that were also found experimentally (Figure 5, Table S3). The oscillator strength of the $S_0 \rightarrow S_1$ transition is large (> 0.9) for all compounds, hinting to a large extinction coefficient for this transition. The second singlet energy level is much higher in energy (> 0.7 eV) in all cases, with the corresponding oscillator strength being negligible, except for dyad **9a** in DMSO and **9c** in all three solvents, where it is very small. There are two triplet states of interest in these BODIPY compounds. The lowest triplet state has an excitation energy of around 1.00 eV for all molecules. The second triplet state is around 2.49 eV for BODIPYs **8a–c** and around 2.24 eV for BODIPYs **9a–c**. According to Kasha's rule, energy transfer from the BODIPY triplet state to the triplet ground state of molecular oxygen should occur from the lowest triplet state.^[43] With an energy of around 1.00 eV, there is still enough energy to overcome the excitation barrier for 3O_2 , which is around 0.98 eV (1270 nm). Based on the calculations, and keeping the possible error on the obtained triplet excitation energies in mind, the lowest triplet state in **9a** and **9c** might be too low in energy for efficient 1O_2 formation, as observed experimentally (Table S3). The dominant nature of the one-particle transitions for the first singlet states is of HOMO \rightarrow LUMO (localized) character. For the second singlet excited state, the character varies between HOMO–1 \rightarrow LUMO (**8a**, **8b** chloroform, **9a**, **9b**, and **9c** DMSO) and HOMO–2 \rightarrow LUMO (**8b** toluene and DMSO, **8c** and **9c** toluene and chloroform) character, depending on the compound and the solvent in which it was calculated, but the nature remains the same, since both HOMO–1 and HOMO–2 are localized on the acridine moiety, leading to a CT-type excitation. For the first and second triplet excited states, the dominant nature is of HOMO \rightarrow LUMO and HOMO–3 \rightarrow LUMO character, respectively.

The CT character of the various transitions was investigated and the distance over which charge is transferred (denoted as d_{CT}) and the change in dipole moment upon excitation were calculated (Table 4). The charge-transfer distance was calculated according to the work by Le Bahers et al.^[44] From the d_{CT} values (< 1.0 Å), it is clear that the $S_0 \rightarrow S_1$, $S_0 \rightarrow T_1$, and $S_0 \rightarrow T_2$ transitions are of local character. On the other hand, the $S_0 \rightarrow S_2$ transition is of CT character ($d_{CT} \geq 1.0$ Å). The change in dipole moment ($\Delta\mu$) follows the same trend: a large increase in dipole moment is observed for $S_0 \rightarrow S_2$, whereas the other transitions show a slight decrease in dipole moment upon excitation. These findings are visualized from the excited state—ground state electron density differences (Figures S6 and S7) and are in line with the picture drawn by the molecular orbitals and natures of the various transitions.

The TDDFT calculations correspond well with the observed localized absorption and emission spectra, in which very little solvatochromism is observed (Figure 5, Table S3). However,

Table 4. Amount of charge-transfer character (d_{CT}) and change in dipole moment ($\Delta\mu$, excited state dipole–ground state dipole) accompanying the $S_0 \rightarrow S_n$ and $S_0 \rightarrow T_n$ transitions in chloroform.

BODIPY	$S_0 \rightarrow S_1$		$S_0 \rightarrow S_2$		$S_0 \rightarrow T_1$		$S_0 \rightarrow T_2$	
	d_{CT} [Å] ^[a]	$\Delta\mu$ [D] ^[b]	d_{CT} [Å] ^[a]	$\Delta\mu$ [D] ^[b]	d_{CT} [Å] ^[a]	$\Delta\mu$ [D] ^[b]	d_{CT} [Å] ^[a]	$\Delta\mu$ [D] ^[b]
8a	0.57	–1.1	4.86	17.8	0.48	–1.2	0.47	–0.7
8b	0.67	–1.4	5.00	18.1	0.65	–1.8	0.38	–0.6
8c	0.79	–1.6	5.13	17.8	0.71	–2.0	0.62	–1.0
9a	0.82	–1.7	4.53	18.1	0.52	–1.5	0.64	–1.2
9b	0.94	–2.0	4.79	19.3	0.71	–2.1	0.62	–1.1
9c	0.99	–2.1	4.93	20.8	0.71	–2.2	0.74	–1.4

[a] Distance over which charge is transferred between the indicated states upon excitation. [b] Dipole moment change upon excitation.

from Table 4, the supposed CT emission as found in dyads **8a** and **8c** in DMSO, and **9a–c** in all solvents, could not be confirmed at the theoretical level. There is indeed an energy level with CT character, but it is much higher in energy than the first singlet state, and not slightly lower as would be expected from the photophysical data, thereby contradicting the observed bathochromically shifted broad band as being a CT band. Furthermore, oscillator strengths are negligible for this transition in all cases. Therefore, another process is expected to be involved in these BODIPY systems.

For SOCT-ISC processes, the Gibbs free-energy change (ΔG_{CS}) can be estimated using the Rehm–Weller equation to check the feasibility of a possible charge separation to form a CT state.^[45] However, for our systems we came across several problems when trying to determine ΔG_{CS} . Although the structural prerequisites seem to be fulfilled in the BODIPY-acridine dyads, TDDFT calculations suggest that no CT state is involved in triplet formation. Furthermore, a definition of the true donor and acceptor parts is troublesome in these systems as the spacer itself also has a donating character and is coplanar with the BODIPY acceptor. Even more, the double bonds can play an important role in terms of the distance between donor and acceptor. Efforts were made to calculate ΔG_{CS} for BODIPYs **8a** and **9a** (see supporting information). To this extent, distyryl-BODIPY **8x** and thienylvinyl-BODIPY **9x** were synthesized and denoted as the electron acceptor components,^[46] whereas 9,9-dimethyl-9,10-dihydroacridine (**4**) was applied as the electron donor. The results seem to point to a possible lower-lying CT state, but can hardly be taken as a solid proof because of the above considerations.

To demonstrate the crucial influence of the acridine end groups on the fluorescence properties and phototoxicity, we compared the photophysical characteristics of dyads **8a** and **9a** with their constituent parts (BODIPY core **7a** and acridine **4**) and the analogous dyes without dimethylacridine moieties (BODIPYs **8x** and **9x**). The absorption and emission profiles, and the extracted data, are given in Figure 6 and Table 5, respectively. Although only two out of the six dyads are discussed here, these results can safely be extrapolated to the other systems.

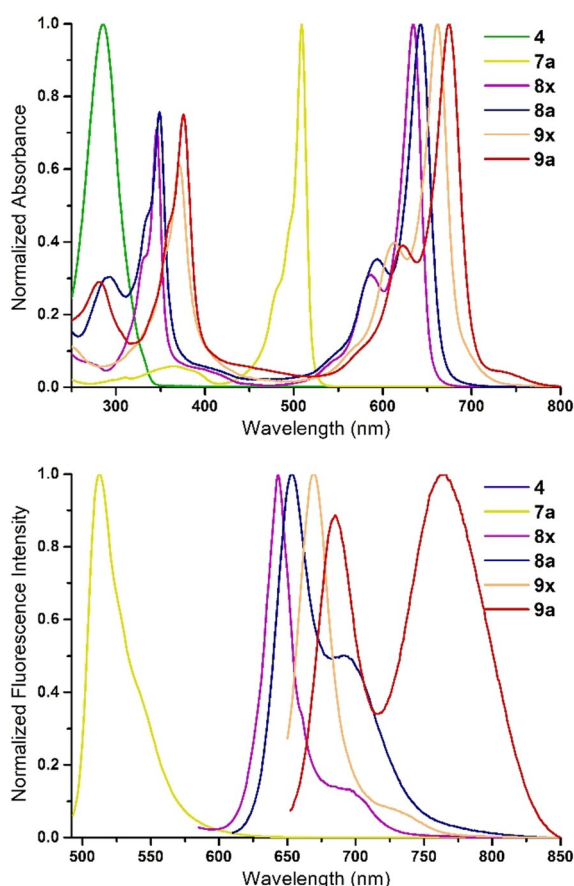


Figure 6. Normalized absorption spectra (top) of **4**, **7a**, **8x**, **9x**, **8a**, and **9a**, and their corresponding normalized fluorescence emission spectra (bottom) in chloroform solution.

Table 5. Spectroscopic data for **4**, **7a**, **8x**, and **9x** as obtained in chloroform solution.^[a]

Compound	λ_{abs} [nm] ^[b]	λ_{em} [nm] ^[c]	$\Delta\tilde{\nu}$ [cm ⁻¹] ^[d]	$fwhm_{\text{abs}}$ [cm ⁻¹] ^[e]	$fwhm_{\text{em}}$ [cm ⁻¹] ^[f]	ϕ_f ^[g]	ϕ_A ^[h]
4	285	457	13 206	5209	2036	0.01	— ^[i]
7a	509	513	153	599	1134	0.96	— ^[i]
8x	634, 346	644	245	1123, 1706	524	0.79	0.01
9x	661, 371	671	225	743, 2336	600	0.50	0.02

[a] Spectrograde chloroform was used for all measurements. [b] Absorption maximum. [c] Fluorescence emission maximum/maxima. [d] Stokes shift between the localized absorption and emission maxima. [e] Full-width-at-half-maximum of the absorption band. [f] Full-width-at-half-maximum of the emission band(s). [g] Fluorescence quantum yield determined vs. 1,4-bis(5-phenyl-2-oxazolyl)benzene ($\lambda_{\text{exc}}=300$ nm, $\phi_f=0.97$ in cyclohexane; for **4**), rhodamine 6G ($\lambda_{\text{exc}}=488$ nm, $\phi_f=0.94$ in ethanol; for **7a**), Cresyl violet ($\lambda_{\text{exc}}=580$ nm, $\phi_f=0.56$ in ethanol; for **8x**), or vs. Nile blue ($\lambda_{\text{exc}}=605$ nm, $\phi_f=0.27$ in ethanol; for **9x**) as a reference. [h] Singlet oxygen quantum yield determined vs. methylene blue ($\phi_A=0.52$, $\lambda_{\text{exc}}=639$ nm) in spectroscopic grade ethanol as a reference by monitoring the absorbance of 1,3-DPBF at 414 nm. [i] Not determined.

The bathochromic shift observed in dyads **8a** and **9a** originates from the increased delocalized system by introducing

the slightly donating styryl and thienylvinyl parts, respectively. This can be seen in BODIPYs **8x** and **9x**, which have typical BODIPY absorption and emission profiles, and maxima red-shifted up to 150 nm as compared to the unmodified BODIPY core **7a**. Introduction of the acridine end groups has only minor effects on these values (≈ 10 nm shift), indicating a disconnection between the acridine and BODIPY parts due to their orthogonality. The additional absorption bands around 350 and 375 nm in **8x/8a** and **9x/9a** can be ascribed to the styryl and vinylthienyl units, respectively. The absorption of the dimethylacridine moiety in **8a** and **9a** is practically unaltered, which is line with the twisted conformation. The fluorescence intensity is expected to decrease compared to BODIPY core **7a**, but is still high in **8x** and moderate in **9x** ($\phi_f=0.79$ and 0.50, respectively). The ϕ_A values remain close to zero in both cases. The reduced fluorescence and low ϕ_A in **9x** indicate an increase in non-radiative losses for materials with a thienyl linker. When acridine **4** is attached, $^1\text{O}_2$ production becomes viable for dyad **8a**. The thirty-fold increase in ϕ_A occurs at the expense of the fluorescence capability, which decreases by 40%. For **9a**, phototoxicity remains low despite the 80% drop in fluorescence emission. Moreover, a second emission band appears. These data clearly indicate the substantial effects of the acridine moieties in our design. Without it, NIR absorption and emission is still possible, but singlet oxygen generation is directly linked to the presence of this additional unit. The absence of the second broad emission band in both **8x** and **9x** is remarkable, indicating it originates from the incorporation of the dimethylacridine structure.

To complete our precursor investigation, DFT and TDDFT calculations were also performed on BODIPYs **8x** and **9x** (Figure S9 and Table S4). In both cases, the first singlet and triplet, and second triplet vertical excitation energies are not altered to a great extent as compared to the excitation energies of **8a** and **9a** (Table 3), which is consistent with the local nature of these transitions. From the positioning of the energy levels, a newly formed singlet state with CT character in **8a** and **9a** arises between the S_1 and S_2 states of **8x** and **9x** when adding the acridine moiety.

Finally, the emission of BODIPYs **8a** and **9a** was investigated at different concentrations. A stock solution was made (ca. 1 mg in 5 mL chloroform), from which a dilution series was derived and emission spectra were recorded (Figure 7). Similar results were obtained in DMSO (Figure S10). Non-normalized fluorescence spectra can be found in Figures S11 and S12. Although only two out of the six dyads are discussed here, these results can likely be extrapolated to the other systems.

In our initial investigation of dyad **9a**, a second broad fluorescence band was observed in chloroform (Figure 4). The same profile is seen at different concentrations, although the relative intensity of the localized emission and the red-shifted band varies. In the most diluted solutions, the fluorescence signal originating from the decay of the ^1LE state is most pronounced. Upon increasing the BODIPY concentration, the broad low-energy band starts to increase in intensity until the point is reached where this band surpasses the LE one. Further increase in concentration decreases the fluorescence intensity

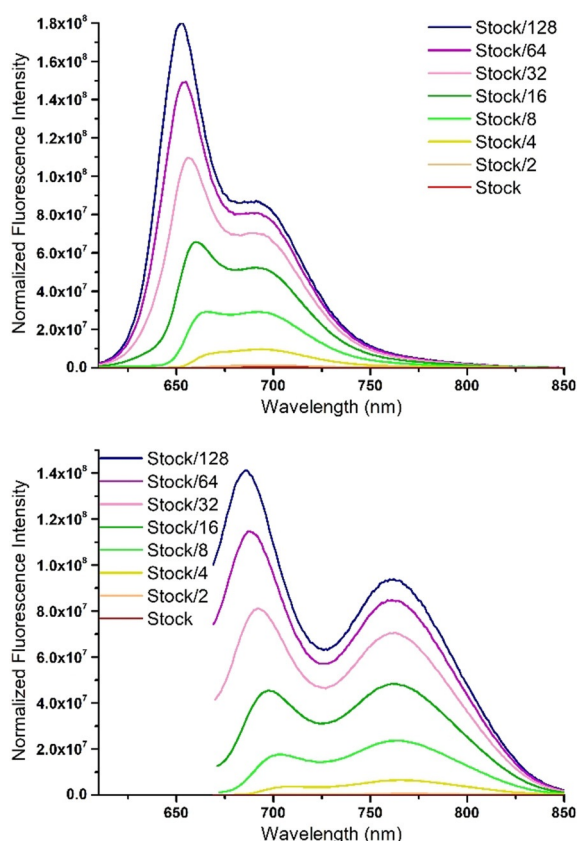


Figure 7. Fluorescence emission spectra, normalized to concentration, for a dilution series of **8a** (top) and **9a** (bottom) in chloroform ($\lambda_{\text{exc}} = 605$ nm, slit width = 2 nm for **8a**; $\lambda_{\text{exc}} = 645$ nm, slit width = 5 nm for **9a**). The stock solution contained ca. 1 mg BODIPY dissolved in 5 mL chloroform.

of both signals, but the localized emission decreases to a greater extent. This concentration dependency suggests the formation of excited state complexes or exciplexes.^[31] Series **9a–c** seems to be very sensitive to exciplex formation as it is perceived in every solvent in diluted solutions. In the ^1H NMR, broad peaks for some of the aromatic protons also confirm the idea of molecular stacking, despite having a seemingly “good” solubility.

BODIPY **8a** exhibits a standard, sharp BODIPY-like emission profile in chloroform (Figure 4). However, looking at different concentrations, it appears there is a second emission band in these systems, originating from a populated exciplex state. Upon increasing concentration, the relative fluorescence intensity of the supposed shoulder increases. At $1/8^{\text{th}}$ of the stock concentration, the red-shifted band becomes more intense than the LE one. In the most concentrated samples, fluorescence is quenched, and the localized emission peak becomes insignificant.

Now the question raises what is the influence of these exciplex states in our systems and, more importantly, in their brightness and phototoxicity? Although the original design was based on a charge recombination induced mechanism, the involvement of a CT state was disputed. As direct ISC from singlet to triplet is unlikely, exciplex formation could be a key element in the ISC abilities. Exciplex states can live relatively

long as there is no ground state counterpart, and they have a strong polar nature, as seen for CT states.^[47] Hence, exciplexes can serve the same purpose as CT states (see energy level scheme in Figure 1), thereby assisting in triplet formation. In the BODIPY-acridine dyads, ISC from a $^1\text{Exciplex}$ state to a ^3LE is questionable. From the TDDFT data (Table 3, Figure S5), it appears that the second ^3LE is even higher in energy than the first ^1LE , and the first ^3LE is too low to be reached directly from the $^1\text{Exciplex}$ state. As an alternative, a $^3\text{Exciplex}$ state should be present to provide ISC, immediately followed by a fast internal conversion to the lowest ^3LE state. In this way, a RP-ISC like mechanism would be obtained. This is a reconcilable statement. The structural double bond results in an increased donor-acceptor distance, thereby decreasing their electronic coupling and reducing the energy splitting between $^1\text{Exciplex}$ and $^3\text{Exciplex}$ states, a feature frequently ascribed to exciplex systems.^[25] Even more, similar ISC behavior into an exciplex triplet state from an excited state complex has already been observed in some BODIPY dyes, although the examples are scarce.^[31,47,48] To fit in the series of other ISC mechanisms, we depicted this alternative as “exciplex intersystem crossing” (EX-ISC).

The photophysical observations from Figure 5 and Table S3 can now be rationalized using the EX-ISC idea. The broad emission observed (**8a–c** in DMSO, **9a–c** in all solvents), was the result of poorly emissive exciplex emission, which explains the low fluorescence quantum yields. The increased back electron transfer hinders triplet formation and thus explains the lack of $^1\text{O}_2$ formation. In toluene and chloroform, only a localized emission peak can be seen in dyads **8a–c** at low concentrations. Due to the polar nature of these exciplex states, its energy will increase in more nonpolar solvents due to its destabilization. In toluene, the energy is too high to allow efficient charge separation from the first singlet excited state, resulting in higher ϕ_f values, but low ϕ_{Δ} . Eventually, in chloroform, it has the ideal position in between the singlet and triplet energy levels. In this way, charge separation can take place in a subtle way to retain localized fluorescence. Furthermore, the $^1\text{Exciplex}$ and $^3\text{Exciplex}$ state are close enough in energy to enable ISC and prevent charge recombination to the ground state. In DMSO, exciplex formation is enhanced as the energy of the exciplex state is lowered, leading to increased charge recombination to the ground state, which is detrimental for the fluorescence and singlet oxygen quantum yields.

Conclusion

For the first time, we have successfully designed and synthesized near-infrared photoactive BODIPY photosensitizers with a high and balanced brightness and phototoxic power for potential use as thera(g)nostic^[1] agents in photodynamic therapy. A large bathochromic shift in the absorption and emission profiles was realized by extending the conjugated system through a fast and simple Knoevenagel condensation strategy. Dimethylacridine moieties were chosen to provide an orthogonal donor-acceptor design in the BODIPY dyads. The structural constraints were confirmed and visualized using density func-

tional theory computational analysis. The acridine moiety was proven to be essential in this design to achieve enhanced triplet population, necessary for singlet oxygen production without the use of heavy atoms. A combination of photophysical studies in solvents of varying polarity at different concentrations and time dependent density functional theory calculations revealed the involvement of exciplex states, which play a crucial role in so-called exciplex intersystem crossing (EX-ISC). Despite their activity deeper into the near-infrared, the BODIPY-acridine dyads connected through a thienyl spacer showed poor fluorescence and singlet oxygen quantum yields. Fortunately, when using a phenyl spacer, fluorescence quantum yields ranging from 38 to 63 % were observed in combination with singlet oxygen quantum yields of 23 to 31 % (in chloroform solution). Further detailed investigations are scheduled to fully understand the excited state deactivation mechanisms taking place. Nevertheless, in combination with their high molar attenuation coefficients, these BODIPY-acridine dyads are very promising for the further development of heavy-atom-free BODIPY photosensitizers active in the phototherapeutic region, combining imaging and the therapeutic process itself for detection and eradication of cancerous cells. Anti-tumor effects and fluorescence optical imaging of our compounds, incorporated in suitable (tumor-targeting) nanoparticle systems, will be pursued in near future as a next step to validate the true potential of this system for theragnostic applications.^[49]

Acknowledgements

The authors thank Hasselt University and the University of Namur for continuing financial support (PhD scholarships J.D. and T.C.). M.K., B.C., and W.M. thank the Research Foundation—Flanders (FWO) for support through project G087718N, Hercules project GOH3816NAUHL, and the Scientific Research Community (WOG) “Supramolecular Chemistry and Materials” (W000620N). The calculations were performed on the computers of the “Consortium des équipements de Calcul Intensif” (CÉCI) (<http://www.ceci-hpc.be>), including those of the “UNamur Technological Platform of High-Performance Computing” (PTCI) (<http://www.ptci.unamur.be>), for which we gratefully acknowledge the financial support from the FNRS-FRFC, the Walloon Region, and the University of Namur (Conventions No. 2.5020.11, GEQ U.G006.15, U.G018.19, 1610468, and RW/GEQ2016).

Conflict of interest

The authors declare no conflict of interest.

Keywords: BODIPY dyes • fluorescence • near-infrared • photosensitizers • singlet oxygen

- [1] S. Frangos, J. R. Buscombe, *Eur. J. Nucl. Med. Mol. Imaging* **2019**, *46*, 519.
[2] a) X. Chen, S. T. C. Wong, *Cancer Theranostics*, Academic Press, Oxford, **2014**; b) S. S. Kelkar, T. M. Reineke, *Bioconjugate Chem.* **2011**, *22*, 1879–

- 1903; c) J. P. Celli, B. Q. Spring, I. Rizvi, C. L. Evans, K. S. Samkoe, S. Verma, B. W. Pogue, T. Hasan, *Chem. Rev.* **2010**, *110*, 2795–2838.
[3] a) X. Li, S. Kolemen, J. Yoon, E. U. Akkaya, *Adv. Funct. Mater.* **2017**, *27*, 1604053; b) B. del Rosal, B. Jia, D. Jaque, *Adv. Funct. Mater.* **2018**, *28*, 1803733; c) C.-N. Ko, G. Li, C.-H. Leung, D.-L. Ma, *Coord. Chem. Rev.* **2019**, *381*, 79–103.
[4] a) T. J. Dougherty, *J. Clin. Laser Med. Surg.* **2002**, *20*, 3–7; b) D. E. Dolmans, D. Fukumura, R. K. Jain, *Nat. Rev. Cancer* **2003**, *3*, 380–387; c) H. v. Tappeiner, *Ergebnisse der Physiologie* **1909**, *8*, 698–741.
[5] a) C. S. Foote, *Photochem. Photobiol.* **1991**, *54*, 659–659; b) S. Kwiatkowski, B. Knap, D. Przystupski, J. Saczko, E. Kedzierska, K. Knap-Czop, J. Kotlinska, O. Michel, K. Kotowski, J. Kulbacka, *Biomed. Pharmacother.* **2018**, *106*, 1098–1107.
[6] A. P. Castano, T. N. Demidova, M. R. Hamblin, *Photodiagn. Photodyn. Ther.* **2004**, *1*, 279–293.
[7] a) J. F. Lovell, T. W. Liu, J. Chen, G. Zheng, *Chem. Rev.* **2010**, *110*, 2839–2857; b) T. J. Dougherty, C. J. Gomer, B. W. Henderson, G. Jori, D. Kessel, M. Korbelik, J. Moan, Q. Peng, *J. Natl. Cancer Inst.* **1998**, *90*, 889–905; c) N. L. Oleinick, R. L. Morris, I. Belichenko, *Photochem. Photobiol. Sci.* **2002**, *1*, 1–21; d) J. M. Dabrowski, L. G. Arnaut, *Photochem. Photobiol. Sci.* **2015**, *14*, 1765–1780.
[8] B. C. Wilson, M. S. Patterson, *Phys. Med. Biol.* **2008**, *53*, R61–R109.
[9] a) J. Moan, K. Berg, *Photochem. Photobiol.* **1991**, *53*, 549–553; b) J. Moan, *J. Photochem. Photobiol. B* **1990**, *6*, 343–344.
[10] a) W. M. Sharman, C. M. Allen, J. E. van Lier, *Drug Discovery Today* **1999**, *4*, 507–517; b) Z. Huang, *Technol. Cancer Res. Treat.* **2005**, *4*, 283–293.
[11] a) M. R. Hamblin, T. Hasan, *Photochem. Photobiol. Sci.* **2004**, *3*, 436–450; b) T. Dai, B. B. Fuchs, J. J. Coleman, R. A. Prates, C. Astrakas, T. G. St Denis, M. S. Ribeiro, E. Mylonakis, M. R. Hamblin, G. P. Tegos, *Front. Microbiol.* **2012**, *3*, 120; c) P. Babilas, S. Schreml, M. Landthaler, R. M. Szeimies, *Photodermatol. Photoimmunol. Photomed.* **2010**, *26*, 118–132; d) M. A. McCormack, *Semin. Cutan. Med. Surg.* **2008**, *27*, 52–62; e) H. I. Pass, *J. Natl. Cancer Inst.* **1993**, *85*, 443–456.
[12] a) T. J. Dougherty, S. L. Marcus, *Eur. J. Cancer* **1992**, *28*, 1734–1742; b) K. Plaetzer, B. Krammer, J. Berlanda, F. Berr, T. Kiesslich, *Lasers Med. Sci.* **2009**, *24*, 259–268.
[13] K. Deng, C. Li, S. Huang, B. Xing, D. Jin, Q. Zeng, Z. Hou, J. Lin, *Small* **2017**, *13*, 1702299.
[14] P. Agostinis, K. Berg, K. A. Cengel, T. H. Foster, A. W. Girotti, S. O. Gollnick, S. M. Hahn, M. R. Hamblin, A. Juzeniene, D. Kessel, M. Korbelik, J. Moan, P. Mroz, D. Nowis, J. Piette, B. C. Wilson, J. Golab, *CA Cancer J. Clin.* **2011**, *61*, 250–281.
[15] A. Juzeniene, K. P. Nielsen, J. Moan, *J. Environ. Pathol. Toxicol. Oncol.* **2006**, *25*, 7–28.
[16] a) R. R. Allison, G. H. Downie, R. Cuenca, X.-H. Hu, C. J. H. Childs, C. H. Sibata, *Photodiagn. Photodyn. Ther.* **2004**, *1*, 27–42; b) M. R. Detty, S. L. Gibson, S. J. Wagner, *J. Med. Chem.* **2004**, *47*, 3897–3915; c) V. Kral, J. Davis, A. Andrievsky, J. Kralova, A. Synytsya, P. Pouckova, J. L. Sessler, *J. Med. Chem.* **2002**, *45*, 1073–1078; d) R. D. Teo, J. Y. Hwang, J. Termini, Z. Gross, H. B. Gray, *Chem. Rev.* **2017**, *117*, 2711–2729; e) S. Swavey, M. Tr, in *Recent Advances in the Biology, Therapy and Management of Melanoma*, **2013**; f) S. J. Wagner, *Transfus. Med. Rev.* **2002**, *16*, 61–66; g) A. E. O'Connor, W. M. Gallagher, A. T. Byrne, *Photochem. Photobiol.* **2009**, *85*, 1053–1074.
[17] R. K. Pandey, *J. Porphyrins Phthalocyanines* **2000**, *04*, 368–373.
[18] a) S. G. Awuah, Y. You, *RSC Adv.* **2012**, *2*, 11169–11183; b) A. Turksoy, D. Yildiz, E. U. Akkaya, *Coord. Chem. Rev.* **2019**, *379*, 47–64; c) L. Yao, S. Xiao, F. Dan, *J. Chem.* **2013**, *2013*, 1–10; d) A. Kamkaew, S. H. Lim, H. B. Lee, L. V. Kiew, L. Y. Chung, K. Burgess, *Chem. Soc. Rev.* **2013**, *42*, 77–88; e) C. S. Kue, S. Y. Ng, S. H. Voon, A. Kamkaew, L. Y. Chung, L. V. Kiew, H. B. Lee, *Photochem. Photobiol. Sci.* **2018**, *17*, 1691–1708; f) L. Huang, G. Han, *Small Methods* **2018**, *2*, 1700370; g) W. Sun, X. Zhao, J. Fan, J. Du, X. Peng, *Small* **2019**, *15*, 1804927; h) M. L. Agazzi, M. B. Ballatore, A. M. Durantini, E. N. Durantini, A. C. Tomé, *J. Photochem. Photobiol. C* **2019**, *40*, 21–48; i) D. Chen, Z. Zhong, Q. Ma, J. Shao, W. Huang, X. Dong, *ACS Appl. Mater. Interfaces* **2020**, *12*, 26914–26925; j) P. Chinna Ayya Swamy, G. Sivaraman, R. N. Priyanka, S. O. Raja, K. Ponnunel, J. Shanmugpriya, A. Gulyani, *Coord. Chem. Rev.* **2020**, *411*, 213233; k) W. Lin, D. Colombani-Garay, L. Huang, C. Duan, G. Han, *WIREs Nanomed. Nanobiotechnol.* **2020**, *12*, e1627.

- [19] a) A. Loudet, K. Burgess, *Chem. Rev.* **2007**, *107*, 4891–4932; b) G. Ulrich, R. Ziessel, A. Harriman, *Angew. Chem. Int. Ed.* **2008**, *47*, 1184–1201; *Angew. Chem.* **2008**, *120*, 1202–1219; c) N. Boens, B. Verbelen, W. Dehaen, *Eur. J. Org. Chem.* **2015**, 6577–6595.
- [20] a) A. B. Descalzo, H. J. Xu, Z. Shen, K. Rurack, *Ann. N. Y. Acad. Sci.* **2008**, *1130*, 164–171; b) Y. Ni, J. Wu, *Org. Biomol. Chem.* **2014**, *12*, 3774–3791; c) H. Lu, J. Mack, Y. Yang, Z. Shen, *Chem. Soc. Rev.* **2014**, *43*, 4778–4823; d) L. Yuan, W. Lin, K. Zheng, L. He, W. Huang, *Chem. Soc. Rev.* **2013**, *42*, 622–661.
- [21] a) J. Zhao, K. Xu, W. Yang, Z. Wang, F. Zhong, *Chem. Soc. Rev.* **2015**, *44*, 8904–8939; b) K. Chen, Y. Dong, X. Zhao, M. Imran, G. Tang, J. Zhao, Q. Liu, *Front. Chem.* **2019**, *7*, 821; c) J. Wang, Q. Gong, L. Wang, E. Hao, L. Jiao, *J. Porphyrins Phthalocyanines* **2020**, *24*, 603–635.
- [22] a) J. Killoran, L. Allen, J. F. Gallagher, W. M. Gallagher, D. F. O'Shea, *Chem. Commun.* **2002**, 1862–1863; b) A. Gorman, J. Killoran, C. O'Shea, T. Kenna, W. M. Gallagher, D. F. O'Shea, *J. Am. Chem. Soc.* **2004**, *126*, 10619–10631; c) T. Yogo, Y. Urano, Y. Ishitsuka, F. Maniwa, T. Nagano, *J. Am. Chem. Soc.* **2005**, *127*, 12162–12163.
- [23] a) E. G. Azenha, A. C. Serra, M. Pineiro, M. M. Pereira, J. Seixas de Melo, L. G. Arnaut, S. J. Formosinho, A. M. d. A. Rocha Gonsalves, *Chem. Phys.* **2002**, *280*, 177–190; b) J. Zou, Z. Yin, K. Ding, Q. Tang, J. Li, W. Si, J. Shao, Q. Zhang, W. Huang, X. Dong, *ACS Appl. Mater. Interfaces* **2017**, *9*, 32475–32481.
- [24] a) J. Zhao, W. Wu, J. Sun, S. Guo, *Chem. Soc. Rev.* **2013**, *42*, 5323–5351; b) J. Zhao, K. Chen, Y. Hou, Y. Che, L. Liu, D. Jia, *Org. Biomol. Chem.* **2018**, *16*, 3692–3701; c) Y. Hou, X. Zhang, K. Chen, D. Liu, Z. Wang, Q. Liu, J. Zhao, A. Barbon, *J. Mater. Chem. C* **2019**, *7*, 12048–12074.
- [25] M. A. Filatov, *Org. Biomol. Chem.* **2020**, *18*, 10–27.
- [26] L. Huang, X. Yu, W. Wu, J. Zhao, *Org. Lett.* **2012**, *14*, 2594–2597.
- [27] a) R. L. Watley, S. G. Awuah, M. Bio, R. Cantu, H. B. Gobeze, V. N. Nesterov, S. K. Das, F. D'Souza, Y. You, *Chem. Asian J.* **2015**, *10*, 1335–1343; b) S. Ji, J. Ge, D. Escudero, Z. Wang, J. Zhao, D. Jacquemin, *J. Org. Chem.* **2015**, *80*, 5958–5963.
- [28] D. Escudero, *Acc. Chem. Res.* **2016**, *49*, 1816–1824.
- [29] a) Z. R. Grabowski, K. Rotkiewicz, W. Rettig, *Chem. Rev.* **2003**, *103*, 3899–4032; b) J. Verhoeven, *J. Photochem. Photobiol. C* **2006**, *7*, 40–60.
- [30] N. Epelde-Elezcano, E. Palao, H. Manzano, A. Prieto-Castaneda, A. R. Agarrabeitia, A. Tabero, A. Villanueva, S. de la Moya, I. Lopez-Arbeloa, V. Martinez-Martinez, M. J. Ortiz, *Chem. Eur. J.* **2017**, *23*, 4837–4848.
- [31] As the exact structures of these “exciplexes” (i.e. excited state complexes) remain unknown for now, we prefer to use this more general term.
- [32] N. Mataga, H. Chosrowjan, S. Taniguchi, *J. Photochem. Photobiol. C* **2005**, *6*, 37–79.
- [33] a) K. Rurack, M. Kollmannsberger, J. Daub, *Angew. Chem. Int. Ed.* **2001**, *40*, 385–387; *Angew. Chem.* **2001**, *113*, 396–399; b) O. Buyukcikir, O. A. Bozdemir, S. Kolemen, S. Erbas, E. U. Akkaya, *Org. Lett.* **2009**, *11*, 4644–4647.
- [34] a) N. A. Kukhta, H. F. Higginbotham, T. Matulaitis, A. Danos, A. N. Bismillah, N. Haase, M. K. Etherington, D. S. Yufit, P. R. McGonigal, J. V. Gražulevičius, A. P. Monkman, *J. Mater. Chem. C* **2019**, *7*, 9184–9194; b) M. Y. Wong, E. Zysman-Colman, *Adv. Mater.* **2017**, *29*, 1605444.
- [35] a) N. Ziebart, P. Schroer, K. Rueck-Braun, *Tetrahedron* **2018**, *74*, 5561–5566; b) Y. Rong, C. Wu, J. Yu, X. Zhang, F. Ye, M. Zeigler, M. E. Gallina, I. C. Wu, Y. Zhang, Y. H. Chan, W. Sun, K. Uvdal, D. T. Chiu, *ACS Nano* **2013**, *7*, 376–384; c) Y. Zhou, Z. Zhou, Y. Li, W. Yang, *Catal. Commun.* **2015**, *64*, 96–100.
- [36] a) Y. Zhao, D. G. Truhlar, *Theor. Chem. Acc.* **2008**, *120*, 215–241; b) J. Tomasi, B. Mennucci, R. Cammi, *Chem. Rev.* **2005**, *105*, 2999–3093.
- [37] a) R. W. Redmond, J. N. Gamlin, *Photochem. Photobiol.* **1999**, *70*, 391–475; b) F. Wilkinson, W. P. Helman, A. B. Ross, *J. Phys. Chem. Ref. Data* **1993**, *22*, 113–262.
- [38] H. Heitele, P. Finckh, S. Weeren, F. Poellinger, M. E. Michel-Beyerle, *J. Phys. Chem.* **1989**, *93*, 5173–5179.
- [39] C. Reichardt, *Chem. Rev.* **1994**, *94*, 2319–2358.
- [40] M. R. Momeni, A. Brown, *J. Chem. Theory Comput.* **2015**, *11*, 2619–2632.
- [41] S. Chibani, B. Le Guennic, A. Charaf-Eddin, A. D. Laurent, D. Jacquemin, *Chem. Sci.* **2013**, *4*, 1950–1963.
- [42] a) D. Jacquemin, E. A. Perpete, I. Ciofini, C. Adamo, *J. Chem. Theory Comput.* **2010**, *6*, 1532–1537; b) C. Brückner, B. Engels, *Chem. Phys.* **2017**, *482*, 319–338.
- [43] M. Kasha, *Discuss. Faraday Soc.* **1950**, *9*, 14–19.
- [44] T. Le Bahers, C. Adamo, I. Ciofini, *J. Chem. Theory Comput.* **2011**, *7*, 2498–2506.
- [45] D. Rehm, A. Weller, *Israel J. Chem.* **1970**, *8*, 259–271.
- [46] H. Kang, Y. Si, Y. Liu, X. Zhang, W. Zhang, Y. Zhao, B. Yang, Y. Liu, Z. Liu, *J. Phys. Chem. A* **2018**, *122*, 5574–5579.
- [47] A. Nano, R. Ziessel, P. Stachelek, M. A. Alamiry, A. Harriman, *ChemPhys-Chem* **2014**, *15*, 177–186.
- [48] A. C. Benniston, G. Copley, H. Lemmetyinen, N. V. Tkachenko, *ChemPhys-Chem* **2010**, *11*, 1685–1692.
- [49] R. Penjweini, S. Deville, L. D'Olieslaeger, M. Berden, M. Ameloot, A. Ethirajan, *J. Controlled Release* **2015**, *218*, 82–93.

Manuscript received: May 25, 2020

Revised manuscript received: June 23, 2020

Accepted manuscript online: June 25, 2020

Version of record online: October 16, 2020